



ORIGINAL ARTICLE

Facile synthesis of the desired red phosphor $\text{Li}_2\text{Ca}_2\text{Mg}_2\text{Si}_2\text{N}_6:\text{Eu}^{2+}$ for high CRI white LEDs and plant growth LED device

Xian Yang¹ | Yu Zhang¹ | Xuejie Zhang¹  | Jian Chen¹ | Haisen Huang¹ | Dongsheng Wang¹ | Xirong Chai¹ | Gening Xie¹ | Maxim S. Molokeyev^{2,3,4} | Haoran Zhang¹ | Yingliang Liu¹ | Bingfu Lei¹ 

¹Guangdong Provincial Engineering Technology Research Center for Optical Agriculture, College of Materials and Energy, College of Horticulture, South China Agricultural University, Guangzhou, China

²Laboratory of Crystal Physics, Kirensky Institute of Physics, Federal Research Center KSC SB RAS, Krasnoyarsk, Russia

³Siberian Federal University, Krasnoyarsk, Russia

⁴Department of Physics, Far Eastern State Transport University, Khabarovsk, Russia

Correspondence

Xuejie Zhang and Bingfu Lei, Guangdong Provincial Engineering Technology Research Center for Optical Agriculture, College of Materials and Energy, South China Agricultural University, Guangzhou 510642, China.

Email: zhangxuejie@scau.edu.cn (X. Z.) and tleibf@scau.edu.cn (B. L.)

Funding information

National Natural Science Foundations of China, Grant/Award Number: 21671070 and 51802101; Project GDUPS; Natural Science Foundation of Guangdong Province, Grant/Award Number: 2018A030310217; Guangzhou Science & Technology Project, Grant/Award Number: 201704030086; Guangdong Provincial Special Fund for Modern Agriculture Industry Technology Innovation Teams; National Undergraduate Innovation and Entrepreneurship Training Program granted for Gening Xie, Grant/Award Number: 201910564035

Abstract

The red emission with suitable peak wavelength and narrow band is acutely required for high color rendering index (CRI) white LEDs without at the cost of the luminous efficacy. Herein, the $\text{Li}_2\text{Ca}_2\text{Mg}_2\text{Si}_2\text{N}_6:\text{Eu}^{2+}$ red phosphor was prepared with facile solid-state method using Ca_3N_2 , Mg_3N_2 , Si_3N_4 , Li_3N , and Eu_2O_3 as the safety raw materials under atmospheric pressure for the first time, which shows red emission peaking at 638 nm with full width at half maximum (FWHM) of 62 nm under blue light irradiation and becomes the desired red phosphor to realize the balance between luminous efficacy and high CRI in white LEDs. The morphology, structure, luminescence properties, thermal quenching behavior, and chromaticity stability of the $\text{Li}_2\text{Ca}_2\text{Mg}_2\text{Si}_2\text{N}_6:\text{Eu}^{2+}$ phosphor are investigated in detail. Concentration quenching occurs when the Eu^{2+} content exceeds 1.0 mol%, whereas high-temperature photoluminescent measurements show a 32% drop from the room-temperature efficiency at 423 K. In view of the excellent luminescence performances of $\text{Li}_2\text{Ca}_2\text{Mg}_2\text{Si}_2\text{N}_6:\text{Eu}^{2+}$ phosphor, a white LEDs with CRI of 91 as a proof-of-concept experiment was fabricated by coating the title phosphor with $\text{Y}_3\text{Al}_5\text{O}_{12}:\text{Ce}^{3+}$ on a blue LED chip. In addition, the potential application of the title phosphor in plant growth LED device was also demonstrated. All the results indicate that $\text{Li}_2\text{Ca}_2\text{Mg}_2\text{Si}_2\text{N}_6:\text{Eu}^{2+}$ is a promising red-emitting phosphor for blue LED-based high CRI white LEDs and plant growth lighting sources.

KEYWORDS

high CRI white LEDs, $\text{Li}_2\text{Ca}_2\text{Mg}_2\text{Si}_2\text{N}_6:\text{Eu}^{2+}$, phosphor, plant growth LED device

1 | INTRODUCTION

To pursue high luminous efficacy and reduce energy consumption caused by low eye sensitivity in the infrared region, red phosphors with suitable peak wavelength and narrow band are urgently needed for high color rendering index (CRI) white LEDs.^{1,2} There is a trade-off between luminous efficacy and high CRI in all types of white LEDs, which means that the improvement in one usually brings about the reduction of the other. The emission peak should be at ~630 nm with relatively narrow band for the optimum balance.^{3,4}

Over the past, nitridosilicate phosphors with excellent luminescence properties and stability as red components were widely utilized in high CRI white LEDs, such as $\text{Sr}_2\text{Si}_5\text{N}_8:\text{Eu}^{2+}$ and $(\text{Ca},\text{Sr})\text{AlSiN}_3:\text{Eu}^{2+}$.^{5,6} However, their broad emissions produce infrared emissions falling out the sensitivity range of the human eye, which leads to the wasted power input and thereby limits the maximum achievable luminous efficacy. The nitridolithoaluminate $\text{SrLiAl}_3\text{N}_4:\text{Eu}^{2+}$ phosphor debuted with peak at ~650 nm and narrow band emission (FWHM = 50 nm) as well as excellent thermal stability, which shows luminous efficacy improvement by 14% compared to commercial phosphor-converted white LEDs (pc-white LEDs).⁷⁻⁹ Unfortunately, a slight redshift of the emission maximum of $\text{SrLiAl}_3\text{N}_4:\text{Eu}^{2+}$ phosphor means a considerable part in spectral regions with low human eye sensitivity not fulfilling requirements of both high CRI and luminous efficacy.^{10,11} Exploration of UCr_4C_4 structure system contributes to the discovery of novel red-emitting nitride phosphor.¹²⁻¹⁵ $\text{CaBaLi}_2\text{Al}_6\text{N}_8:\text{Eu}^{2+}$ derived from $\text{SrLiAl}_3\text{N}_4$ structure with heavier homolog Ba substituting for Sr has been demonstrated to the blueshift of the peak wavelength, it exhibits red emission peaking at 636-639 nm with FWHM of 48-57 nm, as well as another emission peak at 790 nm with FWHM of 89 nm,¹⁶ while the latter emission hinders the enhancement in luminous efficacy. Nitridomagnesosilicates $\text{SrMg}_3\text{SiN}_4:\text{Eu}^{2+}$ phosphor gives a red emission peaking at 615 nm and shows the narrowest emission band (FWHM of 43 nm) up-to-date, but it undergoes serious thermal quenching,^{15,17} hampering its possible applications in pc-white LEDs.

The narrow band red-emitting nitridomagnesosilicate $\text{Li}_2(\text{Ca}_{1-x}\text{Sr}_x)_2\text{Mg}_2\text{Si}_2\text{N}_6:\text{Eu}^{2+}$ ($x = 0-0.06$) was reported by Wolfgang Schnick group in 2017 based on the work of describing the structure of $\text{Li}_2\text{Ca}_2\text{Mg}_2\text{Si}_2\text{N}_6$ compound.¹⁷ $\text{Li}_2\text{Ca}_2\text{Mg}_2\text{Si}_2\text{N}_6:\text{Eu}^{2+}$ shows red emission at 638 nm as well as FWHM of 62 nm under blue light irradiation, which is desirable for high CRI white LEDs.^{18,19} However, the preparation of this phosphor needs the rigorous preparation conditions, such as the sealed tantalum ampules into a silica glass tube, long reaction time more than 90 hours, dangerous raw materials including $\text{Si}(\text{NH})_2$ and LiN_3 . Also, its luminescent properties, thermal quenching behavior, and potential applications in high CRI white LEDs lacks of systematic research.

In this paper, narrow band red-emitting nitride $\text{Li}_2\text{Ca}_2\text{Mg}_2\text{Si}_2\text{N}_6:\text{Eu}^{2+}$ phosphors were prepared using Ca_3N_2 , Mg_3N_2 , Si_3N_4 , Li_3N , and Eu_2O_3 as the safety raw materials under atmospheric pressure for the first time. The morphology, structure, luminescence properties, optimal doped concentration, thermal quenching behavior, and chromaticity stability of the title phosphor are investigated in detail. Employing the title phosphor, commercial $\text{Y}_3\text{Al}_5\text{O}_{12}:\text{Ce}^{3+}$ phosphor, and InGaN-based blue LED chip, a proof-of-concept white LEDs with a CRI of 90 and $R_9 = 90$ is achieved.

Compared with the artificial plant growth LEDs through integrating of red and blue LED chips, the phosphor-converted plant growth LED device exhibits several merits including low cost, facile fabrication, and spectral diversification. However, searching a red phosphor with suitable peak wavelength and narrow band matching well with the absorption spectrum of chlorophyll is acutely required. Thanks to the excellent luminescence performances of $\text{Li}_2\text{Ca}_2\text{Mg}_2\text{Si}_2\text{N}_6:\text{Eu}^{2+}$, in this paper, we also investigated the potential applications of the title red phosphor in plant growth LED device.

2 | EXPERIMENTAL PROCEDURE

2.1 | Preparation of $\text{Li}_2\text{Ca}_2\text{Mg}_2\text{Si}_2\text{N}_6:\text{Eu}^{2+}$ phosphor

The phosphor powders of $\text{Li}_2\text{Ca}_{2-x}\text{Mg}_2\text{Si}_2\text{N}_6:x\text{Eu}^{2+}$ ($x = 0.5\%-4.0\%$) (denoted as $\text{Li}_2\text{Ca}_2\text{Mg}_2\text{Si}_2\text{N}_6:x\text{Eu}^{2+}$) were prepared with the conventional high-temperature solid-state reaction. The raw materials were Ca_3N_2 (99%, purchased from Desunmet Ceramic Material Co., Ltd.), Mg_3N_2 (99.9%, purchased from Desunmet Ceramic Material Co., Ltd.), Si_3N_4 (Aladdin, 99.5%), Li_3N (Alfa Assad, 99.5%), and Eu_2O_3 (Aladdin, 99.99%). The elemental precursors were weighted stoichiometrically and grounded thoroughly using agate mortar and pestle in a nitrogen-filled glove box ($\text{H}_2\text{O} < 1$ ppm, $\text{O}_2 < 1$ ppm). Then, the mixtures were transferred into molybdenum crucibles and fired at 1000°C for 12 hours in a tube furnace under a reducing atmosphere (95% $\text{N}_2/5\%$ H_2).

2.2 | Characterizations

The X-ray powder diffraction were acquired on Rigaku (Cu $K\alpha$ irradiation, 40 kV, 20 mA, $\lambda = 1.5406$ Å). The Rietveld refinement was conducted by TOPAS software. Photoluminescence excitation (PLE) and photoluminescence (PL) spectra were measured with a Hitachi F-7000 fluorescence spectrometer equipped with a 450 W Xenon lamp. Temperature-dependent emission was collected on Hitachi F-7000 fluorescence spectrometer equipped with an Oxford-instruments OptistatDN. Diffuse reflection spectra were measured by UV-Vis-NIR spectrophotometer (SHIMADZU, UV-3600). SEM images and EDS were obtained by an

ultrahigh resolution field-emission scanning electron microscope (FEI, Nova Nano SEM 430).²⁹ Si solid-state NMR spectrum was obtained on Bruker Avance III NMR spectrometer. The optical microscope photographs were required on Zeiss Axio Imager 2. Fluorescence decay curve was recorded on Hamamatsu Quantaurus-Tau C11367 fluorescence spectrophotometer. The electroluminescence (EL) spectra were measured using an integrating sphere (Labsphere) equipped with an Ocean optics spectrograph under an operating forward current.

2.3 | Plant cultivation

Pak-choi cultivation and light expose experiments were conducted under different illumination conditions including present as-prepared plant lamps and the commercial white LEDs lamp. All Pak-choi seedlings were firstly grown under sunlight treatment for 14 days in the outdoor greenhouse, and then the above-mentioned two light sources were used to illuminate the plant for 10 days where the light intensity is $110 \mu\text{mol m}^{-2}\text{s}^{-1}$ photosynthetic photon flux density (PPFD). The illuminate time are from 7:00 to 9:00 at the morning, and 19:00 to 21:00 at night. The cultivation method was hydroponics using Hoagland solution. The Pak-choi without supplementary light treatment was chosen as the reference.

2.4 | Fabrication of White LEDs and plant growth LED device

Prototype white LEDs devices were fabricated using a mixture of epoxy resin, commercial $\text{Y}_3\text{Al}_5\text{O}_{12}:\text{Ce}^{3+}$ phosphor,

with/without the as-prepared $\text{Li}_2\text{Ca}_2\text{Mg}_2\text{Si}_2\text{N}_6:\text{Eu}^{2+}$ phosphor coated on a blue ($\lambda_{\text{em}} = 460 \text{ nm}$) LED chip. The plant growth LED device was fabricated using $\text{Li}_2\text{Ca}_2\text{Mg}_2\text{Si}_2\text{N}_6:\text{Eu}^{2+}$ phosphor and blue LED InGaN chips ($\lambda_{\text{em}} = 455 \text{ nm}$).

3 | RESULTS AND DISCUSSIONS

The XRD pattern of $\text{Li}_2\text{Ca}_2\text{Mg}_2\text{Si}_2\text{N}_6:1.0\%\text{Eu}^{2+}$ sample is shown in Figure 1A and such a pattern is consistent with the standard card apart from several weak peaks of unknown impurity phase. To confirm the structure and estimate the content of impurity, the Rietveld structure refinement for $\text{Li}_2\text{Ca}_2\text{Mg}_2\text{Si}_2\text{N}_6:1.0\%\text{Eu}^{2+}$ was performed and shown in Figure S1, the amount of impurity phase is negligible considering the intensities. The refined structure parameters are also demonstrated in Table S1. The crystal structure of $\text{Li}_2\text{Ca}_2\text{Mg}_2\text{Si}_2\text{N}_6$ is shown in Figure 1B, the network is made up of bow-tie units $[\text{Si}_2\text{N}_6]^{10-}$ which consists of edge sharing double SiN_4 connected by chains of edge sharing MgN_4 . The Ca^{2+} site is in a distorted octahedral coordination surrounded by 6 nitrogen depicted in Figure 1C. The SEM image in Figure 1D shows aggregation and distribution randomly of phosphor particles with size less than $10 \mu\text{m}$. It should be pointed that the phosphor faces the problem of poor water resistance, thus the oxygen content is overestimated. The atomic ratio of phosphor particle is also illustrated in Figure 1E, it reveals an atomic ratio $\text{Ca/Mg/Si} = 1.03:1:1.04$, which agrees well with the formula of $\text{Li}_2\text{Ca}_2\text{Mg}_2\text{Si}_2\text{N}_6$. The ^{29}Si solid-state MAS nuclear magnetic resonance spectrum of $\text{Li}_2\text{Ca}_2\text{Mg}_2$

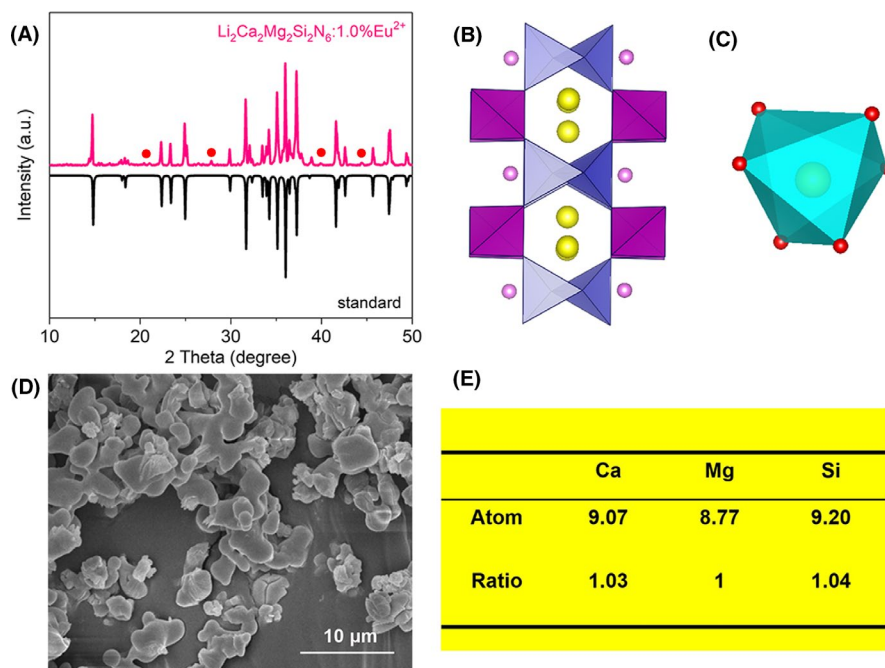


FIGURE 1 A, XRD patterns of standard $\text{Li}_2\text{Ca}_2\text{Mg}_2\text{Si}_2\text{N}_6$ and $\text{Li}_2\text{Ca}_2\text{Mg}_2\text{Si}_2\text{N}_6:1.0\%\text{Eu}^{2+}$ sample, (B) Crystal structure of $\text{Li}_2\text{Ca}_2\text{Mg}_2\text{Si}_2\text{N}_6$. The yellow spheres denote Ca; the pink spheres signify Li; the blue tetrahedrals represent SiN_4 ; the purple tetrahedrals are MgN_4 , (C) Perspective view of the sixfold coordination of Ca^{2+} by six nitrogen, (D) SEM image of $\text{Li}_2\text{Ca}_2\text{Mg}_2\text{Si}_2\text{N}_6:1.0\%\text{Eu}^{2+}$ sample, (E) EDS results (atom%) on the $\text{Li}_2\text{Ca}_2\text{Mg}_2\text{Si}_2\text{N}_6:1.0\%\text{Eu}^{2+}$ phosphor particle [Color figure can be viewed at wileyonlinelibrary.com]

$\text{Si}_2\text{N}_6:1.0\%\text{Eu}^{2+}$ was measured and presented in Figure S2. Mostly, the chemical shift of ^{29}Si is ranging from -40 to -60 ppm in nitrides.^{19–22} There is only one sharp peak observed at -55 ppm, in line with one crystallographic Si site in the structure of $\text{Li}_2\text{Ca}_2\text{Mg}_2\text{Si}_2\text{N}_6$. Considering the crystal structure of $\text{Li}_2\text{Ca}_2\text{Mg}_2\text{Si}_2\text{N}_6$, the peak at -55 ppm could be assigned to the bow-tie units $[\text{Si}_2\text{N}_6]^{10-}$, which also demonstrate that the purity of the sample and no Si-based impurity phase was generated.

UV-Vis diffuse reflectance spectra of host and $\text{Li}_2\text{Ca}_2\text{Mg}_2\text{Si}_2\text{N}_6:1.0\%\text{Eu}^{2+}$ sample are presented in Figure 2. The doped sample shows a broad band absorption in blue to yellow region compared with the undoped sample, which is resulted from the $4f \rightarrow 5d$ transitions of Eu^{2+} ions. The inset presents the digital photograph of $\text{Li}_2\text{Ca}_2\text{Mg}_2\text{Si}_2\text{N}_6:1.0\%\text{Eu}^{2+}$ sample under daylight, it shows light orange body color consistent with its absorption in blue to yellow region. The host and the doped sample show identical absorption band at around 240–280 nm, indicating it is ascribed to the host lattice absorption. The calculated band gap is 4.26 eV (insert of Figure 2) close to the value of 4.6 eV in the literature,¹⁸ illustrating that this compound is an appropriate host for rare earth luminescence.

In the preparation of nitride phosphors, Li_3N usually plays a role as flux to improve the crystallinity.^{21,23} The effect of additional Li_3N concentration on phase and luminescence intensity are shown in Figure S3, which indicates that the excess Li_3N contributes to the crystallinity of the phosphor and the optimal concentration is 120%. The photoluminescence excitation (PLE) and photoluminescence emission (PL) spectra of $\text{Li}_2\text{Ca}_2\text{Mg}_2\text{Si}_2\text{N}_6:1.0\%\text{Eu}^{2+}$ phosphor as well as

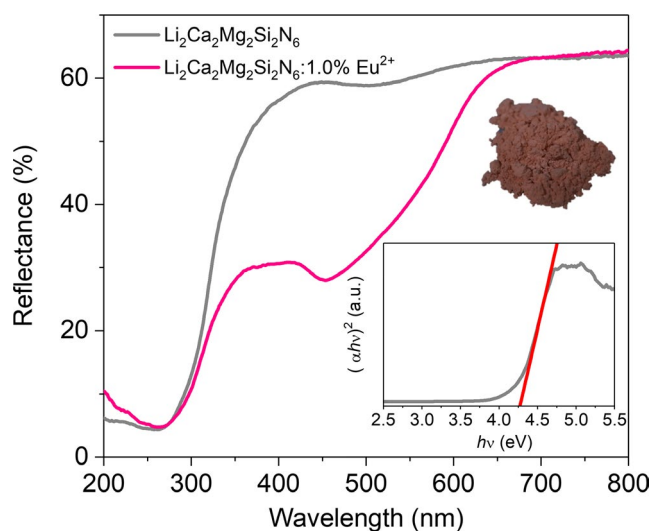


FIGURE 2 Diffuse reflectance spectra of host and $\text{Li}_2\text{Ca}_2\text{Mg}_2\text{Si}_2\text{N}_6:1.0\%\text{Eu}^{2+}$ sample; the inset shows the calculated band gap of $\text{Li}_2\text{Ca}_2\text{Mg}_2\text{Si}_2\text{N}_6:1.0\%\text{Eu}^{2+}$ sample and the digital photograph of $\text{Li}_2\text{Ca}_2\text{Mg}_2\text{Si}_2\text{N}_6:1.0\%\text{Eu}^{2+}$ powder under daylight [Color figure can be viewed at wileyonlinelibrary.com]

$\text{SrLiAl}_3\text{N}_4:\text{Eu}^{2+}$ (as a reference) are shown in Figure 3A. The $\text{Li}_2\text{Ca}_2\text{Mg}_2\text{Si}_2\text{N}_6:1.0\%\text{Eu}^{2+}$ phosphor shows a broad absorption band in blue region, which is consistent with diffuse reflectance spectrum (as demonstrated in Figure 2), indicating it can be efficiently pumped by blue LED chip. Notably, a shoulder band at 530 nm can also be observed. To understand the origin of shoulder band, the PL and PLE spectra at 77 K were collected and presented in Figure S4. The PLE spectrum is obviously different from that at room temperature, which may be due to the phonon-assisted transitions of zero phonon line.^{22,24} Under 460 nm excitation, $\text{Li}_2\text{Ca}_2\text{Mg}_2\text{Si}_2\text{N}_6:1.0\%\text{Eu}^{2+}$ phosphor exhibits the emission peak at 638 nm with FWHM of 62 nm. The powder gives a bright red light under 365 nm UV lamp irradiation (Figure 3A). The emission spectra of $\text{Li}_2\text{Ca}_2\text{Mg}_2\text{Si}_2\text{N}_6:1.0\%\text{Eu}^{2+}$ under different wavelength excitation are also shown in Figure S5. The emission profile is nearly unchanged apart from luminescence intensity due to the difference of absorption value, indicating only one Eu^{2+} crystallographic site exists in $\text{Li}_2\text{Ca}_2\text{Mg}_2\text{Si}_2\text{N}_6$. $\text{SrLiAl}_3\text{N}_4:\text{Eu}^{2+}$ phosphor exhibits an emission band peaking at 650 nm with FWHM of 50 nm under 460 nm excitation (Figure 3A). As above mentioned, the blueshift of narrow band red-emitting phosphor makes a great impact on luminous efficacy of white LEDs device. The most advantage of $\text{Li}_2\text{Ca}_2\text{Mg}_2\text{Si}_2\text{N}_6:1.0\%\text{Eu}^{2+}$ phosphor lies in the position of emission maximum. Compared to $\text{SrLiAl}_3\text{N}_4:\text{Eu}^{2+}$ phosphor, $\text{Li}_2\text{Ca}_2\text{Mg}_2\text{Si}_2\text{N}_6:1.0\%\text{Eu}^{2+}$ gives a short wavelength emission at 638 nm, resulting in less part of emission outside the human eye sensitivity (green dotted line). Differencing from Eu^{2+} ions in a highly symmetric cuboid like environment of $\text{SrLiAl}_3\text{N}_4$ or in highly unusual EuN_9 coordination polyhedron of $\beta\text{-SiAlON}$,^{22,23,25} this compound with distorted octahedral coordination for Eu^{2+} still shows relative narrow band. The possible reason is that the lattice ions like Li, Mg, and Si occupy distinct lattice sites instead of the same lattice site with a statistical distribution, inducing small Stokes shifts and restricting inhomogeneous emission band broadening, thus narrow band occurs.^{24,26} The room-temperature decay curve of $\text{Li}_2\text{Ca}_2\text{Mg}_2\text{Si}_2\text{N}_6:1.0\%\text{Eu}^{2+}$ phosphor under excitation at 460 nm, monitored at the peak of 648 nm is shown in Figure 3B. The lifetime of $\text{Li}_2\text{Ca}_2\text{Mg}_2\text{Si}_2\text{N}_6:1.0\%\text{Eu}^{2+}$ was calculated to be 0.7 μs , which is in line with those determined for other Eu^{2+} -doped nitridosilicate red phosphors, such as $(\text{Ca}/\text{Sr})\text{AlSiN}_3:\text{Eu}^{2+}$ ($\tau = 0.6\text{--}0.8 \mu\text{s}$) and $\text{SrLiAl}_3\text{N}_4:\text{Eu}^{2+}$ ($\tau = 0.6 \mu\text{s}$). The images of phosphor particles were also checked by optical microscope and presented in Figure 3C–D. These particles with the size of 5–10 μm show red emission upon 530-nm green illumination, consistent with the results of emission spectra and SEM images.

Figure 4A–B show the emission spectra and the emission intensity variation of $\text{Li}_2\text{Ca}_{2-x}\text{Mg}_2\text{Si}_2\text{N}_6:x\text{Eu}^{2+}$ ($x = 0.5\%\text{--}4.0\%$) samples under 460 nm excitation. The luminescent intensity is very sensitive to the concentration of

FIGURE 3 A, PLE and PL spectra of $\text{Li}_2\text{Ca}_2\text{Mg}_2\text{Si}_2\text{N}_6:1.0\%\text{Eu}^{2+}$ and $\text{SrLiAl}_3\text{N}_4:\text{Eu}^{2+}$ phosphors; the dotted green curve indicates the upper limit of sensitivity of the human eye; The inset shows the digital photograph of $\text{Li}_2\text{Ca}_2\text{Mg}_2\text{Si}_2\text{N}_6:1.0\%\text{Eu}^{2+}$ phosphor under 365 nm UV lamp; (B) The decay curve of $\text{Li}_2\text{Ca}_2\text{Mg}_2\text{Si}_2\text{N}_6:1.0\%\text{Eu}^{2+}$ under excitation at 460 nm and monitored at 638 nm; Optical microscope images of $\text{Li}_2\text{Ca}_2\text{Mg}_2\text{Si}_2\text{N}_6:1.0\%\text{Eu}^{2+}$ particles in the (C) daylight and (D) upon 530-nm green illumination. [Color figure can be viewed at wileyonlinelibrary.com]

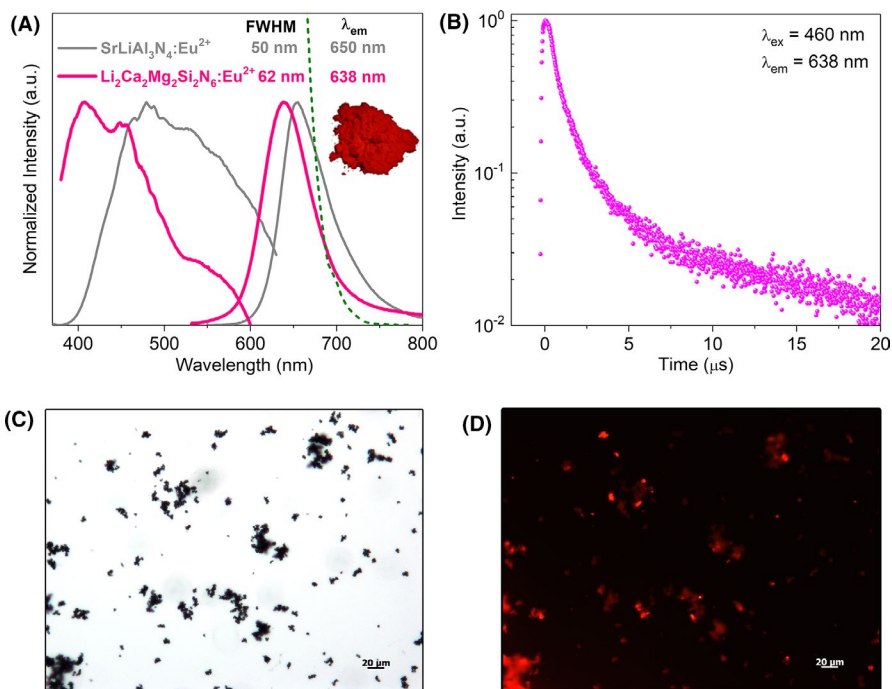
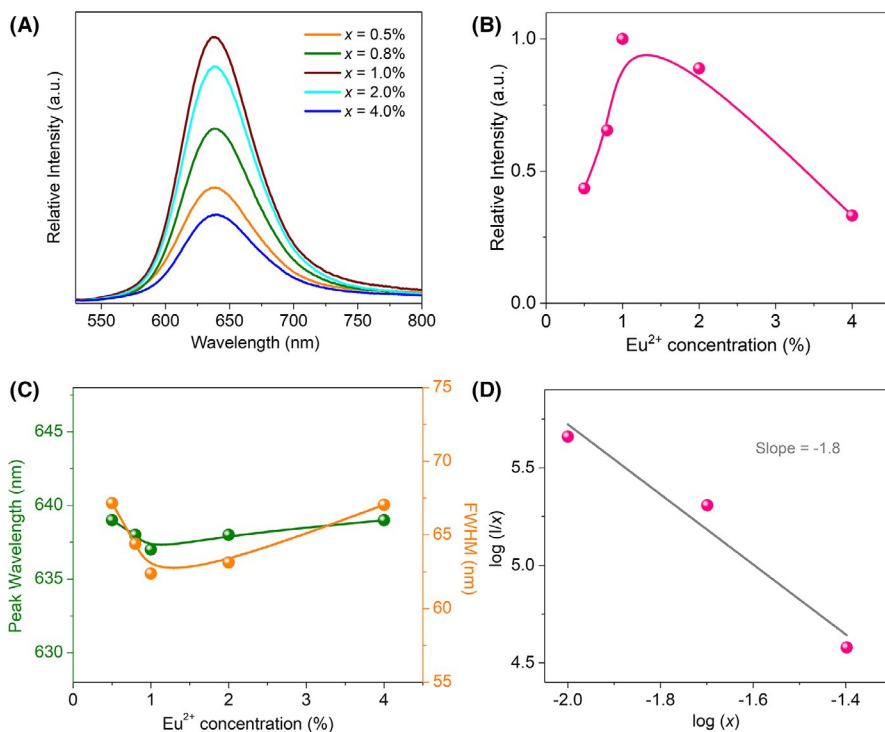


FIGURE 4 A, PL spectra of $\text{Li}_2\text{Ca}_{2-x}\text{Mg}_2\text{Si}_2\text{N}_6:x\text{Eu}^{2+}$ ($x = 0.5\% \sim 4.0\%$); (B) The dependence of peak intensity on Eu^{2+} concentration, (C) The variations of peak wavelengths and FWHM on Eu^{2+} concentration, (D) Relationship between the $\log(I/x)$ and $\log(x)$ of $\text{Li}_2\text{Ca}_2\text{Mg}_2\text{Si}_2\text{N}_6:\text{Eu}^{2+}$ phosphor [Color figure can be viewed at wileyonlinelibrary.com]



Eu^{2+} , determining the optimal Eu^{2+} doping concentration is $x = 1.0\%$, namely the critical concentration. As the concentration of Eu^{2+} increases, the peak wavelength stabilizes in the range of 637–639 nm and the FWHM stabilizes in the range of 62–67 nm. Figure 4D presents the relationship of $\log(x)$ and $\log(I/x)$. The slope is calculated to be -1.8 , indicating the value of θ is 5.4 close to 6. According to Dexter theory,^{25,27} the concentration quenching in $\text{Li}_2\text{Ca}_2\text{Mg}_2\text{Si}_2\text{N}_6:\text{Eu}^{2+}$ phosphors most likely comes from the dipole-dipole interactions.

Thermal stability is of great importance affecting the luminescence performance, it is indispensable to evaluate the thermal quenching behavior and chromaticity stability of phosphor.^{20,26–33} The temperature-dependent PL spectra of $\text{Li}_2\text{Ca}_2\text{Mg}_2\text{Si}_2\text{N}_6:1.0\%\text{Eu}^{2+}$ from room temperature (RT) to 473 K are depicted in Figure 5A–B. With the temperature increasing, the emission intensity gradually decreases attributed to thermal quenching effect and the peak wavelength shows a slight blueshift. Figure 5C illustrates the peak and

integrated intensities of $\text{Li}_2\text{Ca}_2\text{Mg}_2\text{Si}_2\text{N}_6:1.0\%\text{Eu}^{2+}$ with the increase in temperature, respectively. The integrated intensity drops to 87% at 373 K and 68% at 423 K of that initially at RT, respectively. The corresponding peak intensities are 86% and 64%, respectively. The chromaticity shift of $\text{Li}_2\text{Ca}_2\text{Mg}_2\text{Si}_2\text{N}_6:1.0\%\text{Eu}^{2+}$ phosphor with different temperature is presented in Figure 5D. Results indicate that the $\text{Li}_2\text{Ca}_2\text{Mg}_2\text{Si}_2\text{N}_6:1.0\%\text{Eu}^{2+}$ has a good chromaticity stability below 373 K but exhibits an obvious chromaticity shift at high temperature.

The desirable red emission spectra of $\text{Li}_2\text{Ca}_2\text{Mg}_2\text{Si}_2\text{N}_6:1.0\%\text{Eu}^{2+}$ is an attractive candidate for high CRI white LEDs. To demonstrate the potential application of $\text{Li}_2\text{Ca}_2\text{Mg}_2\text{Si}_2\text{N}_6:1.0\%\text{Eu}^{2+}$, the white LEDs (2)

device was fabricated by combining the commercial yellow phosphor ($\text{Y}_3\text{Al}_5\text{O}_{12}:\text{Ce}^{3+}$) with the as-prepared red phosphor on a blue LED chip. And the same time, a commercial white LEDs (1) was also fabricated using a blue LED chip combined with commercial yellow $\text{Y}_3\text{Al}_5\text{O}_{12}:\text{Ce}^{3+}$ phosphor for comparison. The electroluminescence (EL) spectra of the devices under a current of 50 mA current are presented in Figure 6A. The conventional white LEDs (1) encounters high CCT of 7650 K and low CRI of 76, while the CRI of the white LEDs (2) can be improved to 91 and the corresponding CCT decreases to 4226 K with the addition of $\text{Li}_2\text{Ca}_2\text{Mg}_2\text{Si}_2\text{N}_6:\text{Eu}^{2+}$ phosphor. Interestingly, the value of R9 was greatly enhanced to 90, indicating that the red spectral part was enhanced obviously. The color

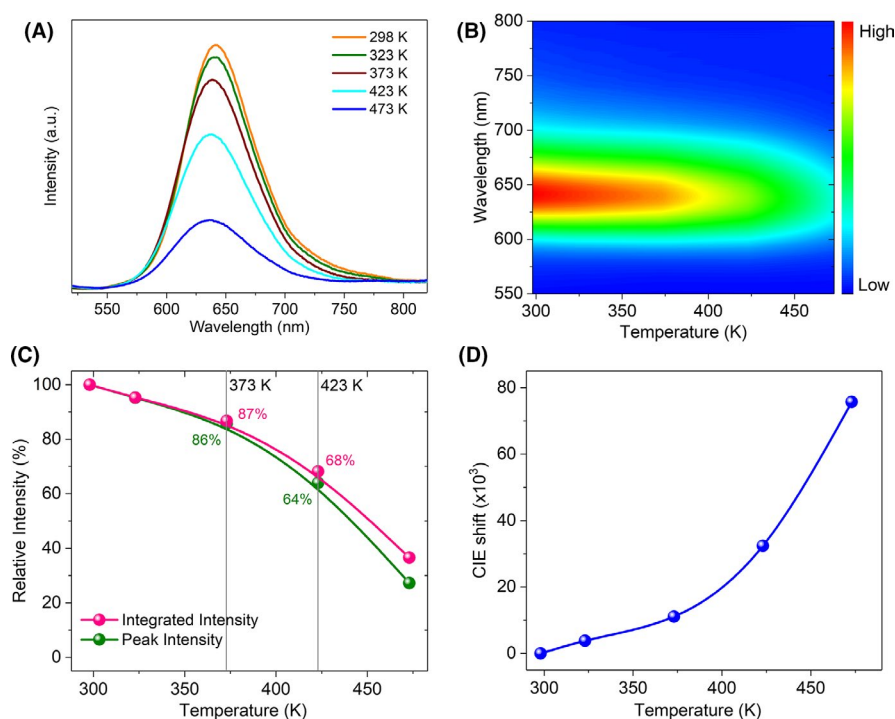


FIGURE 5 A, B, Temperature-dependent PL spectra of $\text{Li}_2\text{Ca}_2\text{Mg}_2\text{Si}_2\text{N}_6:1.0\%\text{Eu}^{2+}$ under 460 nm excitation, (C) Temperature-dependent normalized integrated PL intensities, normalized peak (638 nm) intensities, (D) Chromaticity shift of $\text{Li}_2\text{Ca}_2\text{Mg}_2\text{Si}_2\text{N}_6:\text{Eu}^{2+}$ with different temperature [Color figure can be viewed at wileyonlinelibrary.com]

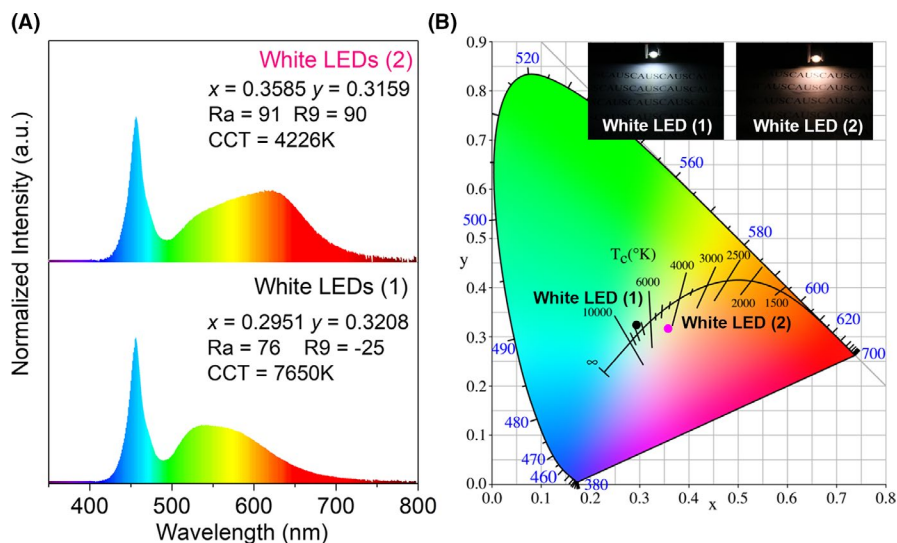


FIGURE 6 A, Electroluminescence spectra of the white LEDs fabricated by a 460-nm blue LED chip, commercial $\text{Y}_3\text{Al}_5\text{O}_{12}:\text{Ce}^{3+}$ phosphor, and as-prepared $\text{Li}_2\text{Ca}_2\text{Mg}_2\text{Si}_2\text{N}_6:1\%\text{Eu}^{2+}$ absent (1) and present (2); (B) Chromaticity coordinates of the two white LEDs, the inset shows photographs of the two white LEDs (1,2) [Color figure can be viewed at wileyonlinelibrary.com]

coordinates and digital photographs of the white LEDs devices are shown in Figure 6B. The light changes from cold white (0.2951, 0.3208) to warm white (0.3585, 0.3159), indicating that $\text{Li}_2\text{Ca}_2\text{Mg}_2\text{Si}_2\text{N}_6:1.0\%\text{Eu}^{2+}$ is a promising candidate material for use in the fabrication of high CRI white LEDs.

Given the suitable peak wavelength and narrow band of $\text{Li}_2\text{Ca}_2\text{Mg}_2\text{Si}_2\text{N}_6:\text{Eu}^{2+}$, it can be a good candidate for plant growth LED device. Hence, red-emitting $\text{Li}_2\text{Ca}_2\text{Mg}_2\text{Si}_2\text{N}_6:\text{Eu}^{2+}$ was coated onto blue LED chips ($\lambda_{\text{em}} = 455 \text{ nm}$) to fabricate a plant growth LED device, which gives the emission matching well with the absorption range of chlorophyll (a or b) (Figure 7C). After being irradiated for 10 days under the same conditions using different light sources (daylight; white LEDs; plant growth LED device), the pak-choi treated by plant growth LED device shows better quality than that illuminated by daylight and white LEDs (Figure 7A-B). The fresh weight, total chlorophyll content, soluble protein content, and total soluble sugar of the pak-choi were analyzed and these results are list in Table 1.^{33,34} All the results indicate that $\text{Li}_2\text{Ca}_2\text{Mg}_2\text{Si}_2\text{N}_6:\text{Eu}^{2+}$ -based plant growth LED device is a suitable light source for enhancing the growth, increasing

the accumulation of nutrients, and promoting photosynthesis in plants.

4 | CONCLUSIONS

In summary, the desired red-emitting $\text{Li}_2\text{Ca}_2\text{Mg}_2\text{Si}_2\text{N}_6:\text{Eu}^{2+}$ phosphors were successfully synthesized by the conventional solid-state method under atmospheric pressure. With the XRD, SEM, PLE and PL, and NMR measurements, the phase, morphology, luminescence properties, and the structure of phosphor were systematically studied. The $\text{Li}_2\text{Ca}_2\text{Mg}_2\text{Si}_2\text{N}_6:\text{Eu}^{2+}$ phosphor with a broad absorption in blue to yellow region shows red emission peaking around 638 nm with FWHM of 62 nm, which is desirable pursuit for the balance of luminous efficacy and CRI. The aid-sintering additive of Li_3N contributes to the crystallinity and enhances luminescence intensity. The title phosphor shows good thermal quenching behavior that the integrated intensity can remain 68% of the pristine even heating up to 423 K and the quenching of emission intensity occurs when the doping concentration of Eu^{2+} exceeds 1.0%. Moreover, the warm white with low CCT (4224 K) and high CRI (91) could be garnered

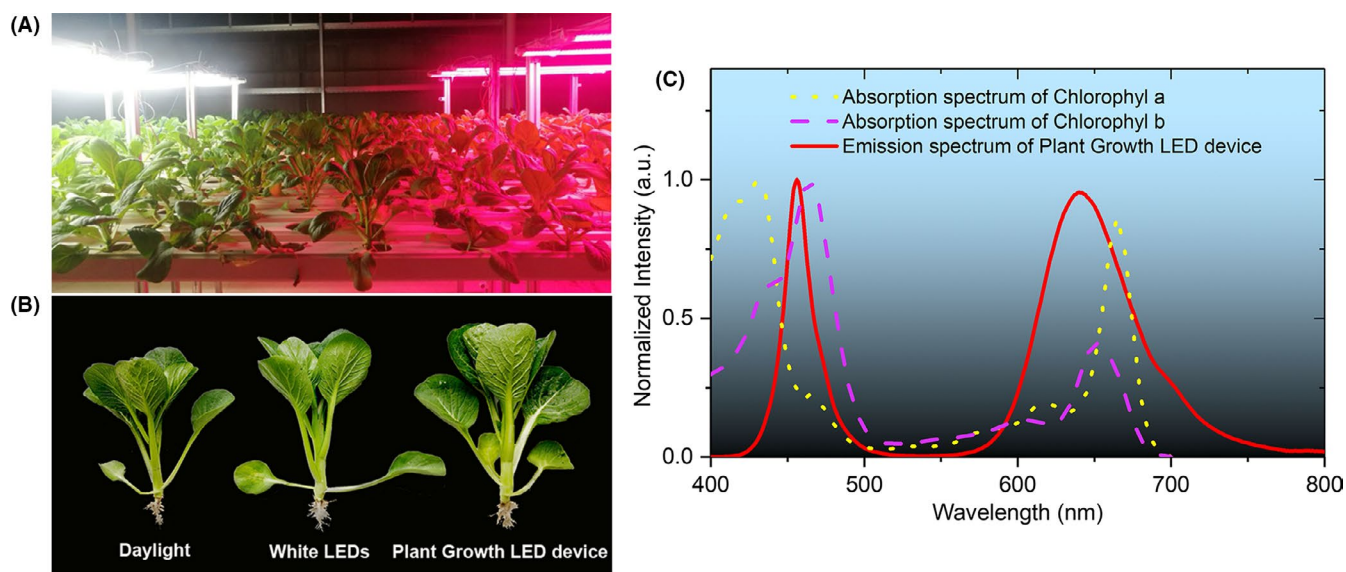


FIGURE 7 A, Indoor pak-choi cultivation irradiated by different lighting sources; (B) Digital photographs of pak-choi cultivation irradiated by different lighting sources; (C) Absorption spectra of Chlorophyll (a and b) and the emission spectrum of $\text{Li}_2\text{Ca}_2\text{Mg}_2\text{Si}_2\text{N}_6:1.0\%\text{Eu}^{2+}$ -based plant growth LED device [Color figure can be viewed at wileyonlinelibrary.com]

TABLE 1 Effect of different light sources on the indicators of pak-choi (a-c represent daylight, white LEDs, and plant growth LED device, respectively)

Fresh weight (g plant^{-1})	Total chlorophyll content ($\mu\text{g g}^{-1}$)	Soluble protein content (mg g^{-1})	Total soluble sugar (mg g^{-1})
32.09	764.2	4.80	1.29
35.74	836.8	7.69	1.95
38.22	1073.7	6.82	2.49

through combining the title phosphor and yellow-emitting $\text{Y}_3\text{Al}_5\text{O}_{12}:\text{Ce}^{3+}$ in blue LED chip. These results demonstrate that $\text{Li}_2\text{Ca}_2\text{Mg}_2\text{Si}_2\text{N}_6:\text{Eu}^{2+}$ has a great potential to serve as the desired red light component applied in high CRI white LEDs. The further study in indoor pak-choi cultivation experiment also indicates that $\text{Li}_2\text{Ca}_2\text{Mg}_2\text{Si}_2\text{N}_6:\text{Eu}^{2+}$ red phosphor is a promising material applied in plant growth.

ACKNOWLEDGMENTS

This work was financially supported by the National Natural Science Foundations of China (Grant Nos. 21671070, 51802101), the Project GDUPS (2018) for B. Lei, the Natural Science Foundation of Guangdong Province (No. 2018A030310217), the Guangzhou Science & Technology Project (No. 201704030086), the Guangdong Provincial Special Fund for Modern Agriculture Industry Technology Innovation Teams, and the National Undergraduate Innovation and Entrepreneurship Training Program granted for Gening Xie (No. 201910564035).

ORCID

Xuejie Zhang  <https://orcid.org/0000-0002-4029-7000>

Bingfu Lei  <https://orcid.org/0000-0002-6634-0388>

REFERENCES

- Pust P, Schmidt PJ, Schnick W. A revolution in lighting. *Nat Mater.* 2015;14:454–8.
- Wang L, Xie R-J, Li Y, Wang X, Ma C-G, Luo D, et al. $\text{Ca}_{1-x}\text{Li}_x\text{Al}_{1-x}\text{Si}_{1+x}\text{N}_3:\text{Eu}^{2+}$ solid solutions as broadband, color-tunable and thermally robust red phosphors for superior color rendition white light-emitting diodes. *Light-Sci Appl.* 2016;5:16155–63.
- Xia Z, Liu Q. Progress in discovery and structural design of color conversion phosphors for LEDs. *Prog Mater Sci.* 2016;84:59–117.
- Wang L, Xie R-J, Suehiro T, Takeda T, Hirosaki N. Down-conversion nitride materials for solid state lighting: recent advances and perspectives. *Chem Rev.* 2018;118:1951–2009.
- Xie R-J, Hirosaki N, Suehiro T, Xu F, Mitomo M. A simple, efficient synthetic route to $\text{Sr}_2\text{Si}_3\text{N}_8:\text{Eu}^{2+}$ -based red phosphors for white light-emitting diodes. *Chem Mater.* 2006;18:5578–83.
- Zhu J, Wang L, Zhou T, Cho Y, Suehiro T, Takeda T, et al. Moisture-induced degradation and its mechanism of $(\text{Sr}, \text{Ca})\text{AlSiN}_3:\text{Eu}^{2+}$, a red-color-converter for solid state lighting. *J Mater Chem C.* 2015;3:3181–8.
- Pust P, Weiler V, Hecht C, Tücks A, Wochnik AS, Hen A, et al. Narrow-band red-emitting $\text{Sr}[\text{LiAl}_3\text{N}_4]:\text{Eu}^{2+}$ as a next-generation LED-phosphor material. *Nat Mater.* 2014;13:891–6.
- Cui D, Xiang Q, Song Z, Xia Z, Liu Q. The synthesis of narrow-band red-emitting $\text{SrLiAl}_3\text{N}_4:\text{Eu}^{2+}$ phosphor and improvement of its luminescence properties. *J Mater Chem C.* 2016;4:7332–8.
- Zhang X, Yu J, Wang J, Zhu C, Zhang J, Zou R, et al. Facile preparation and ultrastable performance of single-component white-light-emitting phosphor-in-glass used for high-power warm white LEDs. *ACS Appl Mater Interfaces.* 2015;7:28122–7.
- Lin CC, Meijerink A, Liu R-S. Critical red components for next-generation white LEDs. *J Phys Chem Lett.* 2016;7:495–503.
- Li W, Song Z, Cui D, Xia Z, Liu Q. Moisture-induced degradation of the narrow-band red-emitting $\text{SrLiAl}_3\text{N}_4:\text{Eu}^{2+}$ phosphor. *J Rare Earth.* 2018;36:341–5.
- Pust P, Hintze F, Hecht C, Weiler V, Locher A, Zitnanska D, et al. Group (III) Nitrides $\text{M}[\text{Mg}_2\text{Al}_2\text{N}_4]$ ($\text{M} = \text{Ca}, \text{Sr}, \text{Ba}, \text{Eu}$) and $\text{Ba}[\text{Mg}_2\text{Ga}_2\text{N}_4]$ —structural relation and nontypical luminescence properties of Eu^{2+} doped samples. *Chem Mater.* 2014;26:6113–9.
- Pust P, Wochnik AS, Baumann E, Schmidt PJ, Wiechert D, Scheu C, et al. $\text{Ca}[\text{LiAl}_3\text{N}_4]:\text{Eu}^{2+}$ —a narrow-band red-emitting nitridolithoaluminate. *Chem Mater.* 2014;26:3544–9.
- Schmiechen S, Strobel P, Hecht C, Reith T, Siegert M, Schmidt PJ, et al. Nitridomagnesiumsilicate $\text{Ba}[\text{Mg}_3\text{SiN}_4]:\text{Eu}^{2+}$ and structure–property relations of similar narrow-band red nitride phosphors. *Chem Mater.* 2015;27:1780–5.
- Schmiechen S, Schneider H, Wagatha P, Hecht C, Schmidt PJ, Schnick W. Toward new phosphors for application in illumination-grade white pc-LEDs: the nitridomagnesiumsilicates $\text{Ca}[\text{Mg}_3\text{SiN}_4]:\text{Ce}^{3+}$, $\text{Sr}[\text{Mg}_3\text{SiN}_4]:\text{Eu}^{2+}$, and $\text{Eu}[\text{Mg}_3\text{SiN}_4]$. *Chem Mater.* 2014;26:2712–9.
- Wagatha P, Weiler V, Schmidt PJ, Schnick W. Tailoring emission characteristics: narrow-band red luminescence from SLA to $\text{CaBa}[\text{Li}_2\text{Al}_6\text{N}_8]:\text{Eu}^{2+}$. *Chem Mater.* 2018;30:7885–91.
- Schmiechen S, Nietschke F, Schnick W. Structural relationship between the Mg-containing nitridosilicates $\text{Ca}_2\text{Mg}[\text{Li}_4\text{Si}_2\text{N}_6]$ and $\text{Li}_2\text{Ca}_2[\text{Mg}_2\text{Si}_2\text{N}_6]$. *Eur J Inorg Chem.* 2015;9:1592–7.
- Strobel P, Weiler V, Hecht C, Schmidt PJ, Schnick W. Luminescence of the narrow-band red emitting nitridomagnesiumsilicate $\text{Li}_2(\text{Ca}_{1-x}\text{Sr}_x)_2[\text{Mg}_2\text{Si}_2\text{N}_6]:\text{Eu}^{2+}$ ($x = 0–0.06$). *Chem Mater.* 2017;29:1377–83.
- Stadler F, Oeckler O, Senker J, Höpfe HA, Kroll P, Schnick W. SrSi_6N_8 —a reduced nitridosilicate with a Si-Si Bond. *Angew Chem Inter Edition.* 2005;44:567–70.
- Stadler F, Schnick W. The new layer-silicates $\text{Ba}_3\text{Si}_6\text{O}_9\text{N}_4$ and $\text{Eu}_3\text{Si}_6\text{O}_9\text{N}_4$. *Z Anorg Allg Chem.* 2006;2632:949–54.
- Hu W, Ji W, Khan SA, Hao L, Xu X, Yin L, et al. Preparation of $\text{Sr}_{1-x}\text{Ca}_x\text{LiAl}_3\text{N}_4:\text{Eu}^{2+}$ solid solutions and their photoluminescence properties. *J Am Ceram Soc.* 2016;99:3273–9.
- Zhang X, Fang MH, Tsai YT, Lazarowska A, Mahlik S, Lesniewski T, et al. Controlling of structural ordering and rigidity of β - $\text{SiAlON}:\text{Eu}$ through chemical cosubstitution to approach narrow-band emission for light-emitting diodes application. *Chem Mater.* 2017;29:6781–92.
- Tsai YT, Chiang CY, Zhou W, Lee JF, Sheu HS, Liu R-S. Structural ordering and charge variation induced by cation substitution in $(\text{Sr}, \text{Ca})\text{AlSiN}_3:\text{Eu}$ phosphor. *J Am Chem Soc.* 2015;137:8936–9.
- Li S, Xie R-J, Takeda T, Hirosaki N. Review-narrow-band nitride phosphors for wide color-gamut white LED backlighting. *ECS J Solid State Sci Technol.* 2018;7:3064–78.
- Dexter DL, Schulman JH. Theory of concentration quenching in inorganic phosphors. *J Chem Phys.* 1954;22:1063–70.
- Wei Y, Cao L, Lv L, Li G, Hao J, Gao J, et al. Highly efficient blue emission and superior thermal stability of $\text{BaAl}_{12}\text{O}_{19}:\text{Eu}^{2+}$ phosphors based on highly symmetric crystal structure. *Chem Mater.* 2018;30:2389–99.

27. Deng J, Zhang H, Zhang X, Molokeev MS, Qiu J, Liu Y, et al. Enhanced luminescence performance of CaO:Ce³⁺, Li⁺, F⁻ phosphor and its phosphor-in-glass based high-power warm LED properties. *J Mater Chem C*. 2018;6:4077–86.
28. Guo H, Zheng Z, Teng L, Wei R, Hu F. Tunable white-light emission and energy transfer in single-phase Bi³⁺, Eu³⁺ co-doped Ba₉Y₂Si₆O₂₄ phosphors for UV w-LEDs. *J Lumin*. 2019;213:494–503.
29. Long Z, Wen Y, Qiu J, Wang J, Zhou D, Zhu C, et al. Crystal structure insight aided design of SrGa₂Si₂O₈:Mn²⁺ with multi-band and thermally stable emission for high-power LED applications. *Chem Eng J*. 2019;122016.
30. Xia L, Yue Y, Yang X, Deng Y, Li C, Zhuang Y, et al. Facile preparation and optical properties of Te/Pb-free Y₃Al₅O₁₂:Ce³⁺ phosphor-in-glass via a screen-printing route for high-power WLEDs. *J Eur Ceram Soc*. 2019;39:3848–55.
31. Guo H, Zhang H, Li J, Li F. Blue-white-green tunable luminescence from Ba₂Gd₂Si₄O₁₃:Ce³⁺, Tb³⁺ phosphors excited by ultraviolet light. *Opt Express*. 2010;18:27252–62.
32. Long Z, Wen Y, Zhou J, Qiu J, Wu H, Xu X, et al. No-interference reading for optical information storage and ultra-multiple anti-counterfeiting applications by designing targeted recombination in charge carrier trapping phosphors. *Adv Opt Mater*. 2019;7:1900006.
33. Deng J, Zhang H, Zhang X, Zheng Y, Yuan J, Liu H, et al. Ultrastable red-emitting phosphor-in-glass for superior high-power artificial plant growth LEDs. *J Mater Chem C*. 2018;6:1738–45.
34. Li M, Zhang X, Zhang H, Chen W, Ma L, Wang X, et al. Highly efficient dual broad emitting light convertor: an option for next-generation plant growth LEDs. *J Mater Chem C*. 2019;7:3617–22.

SUPPORTING INFORMATION

Additional supporting information may be found online in the Supporting Information section.

How to cite this article: Yang X, Zhang Y, Zhang X, et al. Facile synthesis of the desired red phosphor Li₂Ca₂Mg₂Si₂N₆:Eu²⁺ for high CRI white LEDs and plant growth LED device. *J Am Ceram Soc*. 2020;103:1773–1781. <https://doi.org/10.1111/jace.16858>